# AN INITIAL QUANTITATIVE COMPARATIVE STUDY OF THE CONTRAST RESOLUTION OF DIFFERENT ULTRASOUND IMAGING TRANSDUCERS

K.A. Micallef, M.L. Camilleri

University of Malta, Msida, Malta

*Abstract* – **The current established guidelines to assess the contrast resolution in ultrasound (US) systems suggest that tests are done qualitatively. To limit subjectivity, various quantitative methods were investigated to analyse the contrast resolution across different US transducers, frequencies and depths. This includes the index contrast (IC), the gamma of the system, and the contrast-to- noise ratio (CNR). From the data gathered by using the CIRS Model 040GSE phantom and ImageJ, it was found that the IC increases with hyperechoic structures, for all transducer types. Regarding the gamma values, it was found that it depends on the type of transducers and not on the frequency whilst for the CNR, all transducer types established characteristic U-shaped scatter plots. Through these methods, it was concluded that the sector probes established better performance at the near and far field zones. Moreover, from most data plotted, it was found that the contrast resolution is not frequency- dependent.**

*Keywords- ultrasound, contrast resolution, quantitative methods, transducers, probes, quality assurance, quality control*

## I. INTRODUCTION

US imaging is a non-ionising radiation modality which can be used for real-time assessments of foetal development and tumour diagnosis in abdominal organs, Lanzolla et al. (2011). As thoroughly highlighted by Lanzolla et al. (2011), US images can be obtained using various modes. For this study, the brightness display mode (B-mode) was utilised where the brightness of a 2D greyscale image is proportional to the signal amplitude.

This research study addresses the problem of how contrast resolution in diagnostic US modalities is assessed. Standards and published documents, such as reports from the IPEM and the AAPM, recommend that contrast resolution should be measured visually using scoring methods. This subjective approach results in less efficient quality assurance (QA) and quality control (QC) testing when monitoring the contrast resolution of different US systems and probes.

In light of this, the need to develop a quantitative method will provide a clear understanding of the contrast resolution behaviour across different probes, depths and frequencies. Based on the current literature, different ways to analyse contrast resolution are present. This study had the following objectives:

- To develop a quantitative approach to investigate and assess contrast resolution.
- To analyse the behaviour of contrast resolution of different transducers: linear, curvilinear and sector.
- To investigate contrast resolution for different frequencies.
- To understand the behaviour of contrast resolution at different depths.

To investigate the above, various greyscale images from acceptance testing were acquired as part of the data collection. Then, using ImageJ and Microsoft Excel Version 16.86, data was extracted and analysed.

### A. Contrast Resolution

Contrast resolution is defined as "the ability of the US imaging system to detect subtle differences in the echogenicity of two targets" (Sarassoli et al., 2019). Multiple studies investigated this parameter, considering different phantoms and software programmes along with various probes operating at different frequencies. The probes include the ones shown in Fig. 1.

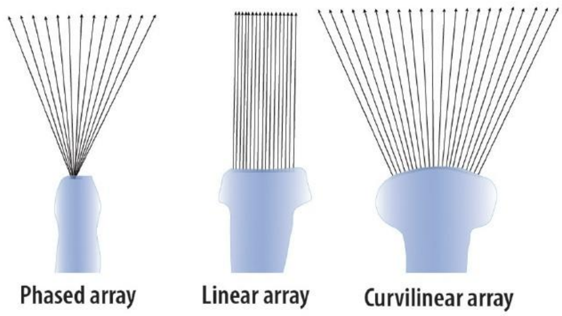


Fig. 1. (2021) Diagram of the Transducers FOV, Vanderland and Kumar

### B. International Standards

For the contrast resolution or the greyscale performance test, the IPEM 102 report mentions that it can be tested by imaging a section within the phantom with different echoic targets ranging from hypoechoic to hyperechoic. In this way, each target would be subjectively analysed by using a 3-point scale rating as defined through Table I.

Table I: Lesion target scoring based on IPEM 102

| IPEM 102 - Lesion Target Scoring - 3-Point Scale | |
|---|---|
| Score 1 | Not seen |
| Score 2 | Seen but distinct |
| Score 3 | Clearly seen |

On the other hand, even though AAPM does not have a specific protocol for assessing the greyscale performance of an US system, it emphasises its importance within a comprehensive QC procedure. Moreover, AAPM suggests that consistent greyscale performance is crucial for comparing US systems and probes over time.

# II. MATERIALS AND METHODOLOGY

## *A. Data Collection Technique*

Images were gathered from various acceptance tests which were performed over four years. For images to be obtained, a Standard Operating Procedure (SOP) based on IPEM 102 was followed to ensure that testing on the contrast resolution is conducted as suggested in these guidelines. Using a dedicated phantom, such guidelines allowed different US transducers to be tested on various US devices available at Mater Dei Hospital (MDH).

The ultrasound images collected retrospectively were saved in Digital Imaging and Communications in Medicine (DICOM) format to be further evaluated through ImageJ. Through this chosen software, the images saved from the US systems were investigated, allowing quantitative data to be extracted and gathered.

With the use of a TETO and coupling gel, the linear, curvilinear, and sector probes were tested on various US systems. Endocavity/endovaginal and hockey-stick type probes were also assessed. For the contrast resolution to be analysed through the system's greyscale performance, the following steps were considered to obtain an optimised US image:

1) The dedicated phantom was scanned by applying coupling gel on the phantom area which has an attenuating material 0.5 dB/(cm·MHz), as shown in Fig. 2.
2) With the transducer under test, the first set of different grey cylindrical targets was scanned. A total of six targets; -9 dB, -6 dB, -3 dB, +3 dB, +6 dB and +15 dB were imaged at a depth of 3 cm within the phantom.
3) Upon scanning the TETO, the image was optimised by ensuring that contrast between the speckle background and the target is achieved. This was achieved by adjusting the Amplification Gain, Time-Gain Compensation (TGC) and by setting the focus at the greyscale targets set.
4) The image/s of the cylindrical targets located at this depth were saved and exported in DICOM format, as shown in Fig. 3, for further analysis on ImageJ.
5) The above steps were repeated for the other five different grey cylindrical targets located at a depth of 11.5 cm. At this depth, the -6 dB, -3 dB, +3 dB, +6 dB and +15 dB targets were tested.


Fig. 2. Scanning the CIRS Model 040GSE TETO, CIRS (n.d.)

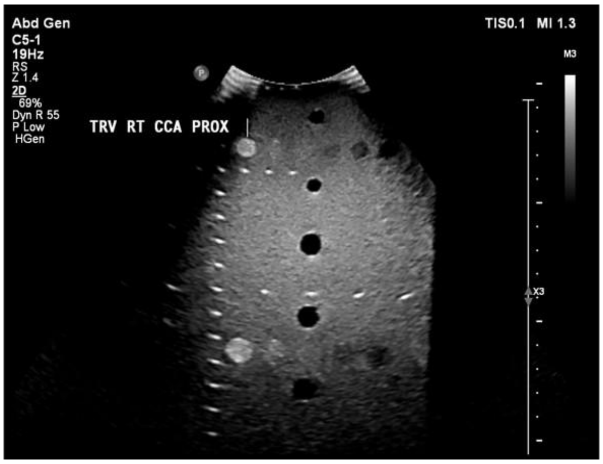


Fig. 3. An US image using a curvilinear transducer on the Philips EPIQ Elite 5G system

## *B. Data Collection Tool*

As shown in Table II, 21 US systems equipped with 52 probes were tested. The probes are further classified into 17 linear, 20 curvilinear and 15 sector. For these to be evaluated, the CIRS Model 040GSE TETO shown in Fig. 4 was used together with the ImageJ software for data analysis.

Table II: A table of all the US systems and probes assessed

| Probe Details | | | | |
|---|---|---|---|---|
| **Manufacturer** | **Model** | **Linear** | **Curvilinear** | **Sector** |
| Philips | Sparq | L12-4 | C5-1 | S5-1 |
| | Affiniti 30 | - | C6-2 | - |
| | Epiq Cardiac CVx 3D | - | - | X5-1 |
| | | - | - | X7-2 |
| | | - | - | S8-3 |
| | | - | - | S12-4 |
| | Lumify 72 SMT-T590 | - | - | S4-1 |
| | Lumify 91 SMT-T590 | - | C5-2 | - |
| | Lumify 86 SMT-T590 | L12-4 | - | - |
| | Lumify 87 SMT-T590 | L12-4 | - | - |
| | Lumify 89 SMT-T590 | - | - | S4-1 |
| | EPIQ Elite 5G | L12-3 | C5-1 | - |
| | | L15-7io | - | - |
| | CS50 POC | L12-3 | C5-1 | - |
| Canon | Aplio i800 | i18LX5 | - | - |
| | Aplio a550 | - | 8C1 | - |
| | Aplio a450 | - | 6C1 | - |
| | | - | 11C3 | - |
| | Aplio a | - | 8C1 | - |
| | | 11CL4-LA | 11CL4-CA | - |
| Toshiba | Aplio300 | 14L5 | 6C1 | - |
| | Aplio a400 | - | 6C1 | - |
| | Aplio 500 | 14L5 | - | - |
| GE | Vivid iQ | 12L-RS | - | - |
| | Voluson S6 | - | EndoVaginal | - |
| | Voluson S10 | - | Transvaginal I9-RS | - |
| Esaote | X7 | L4-15 | - | - |

## C. Data Analysis Technique

The data analysis techniques used were based on what was commonly implemented in the literature. For this reason, three particular methods were investigated. These include the evaluation of the gamma of the system, the IC and the CNR. All of these approaches were considered to provide a better insight into the US system and probe's overall performance.

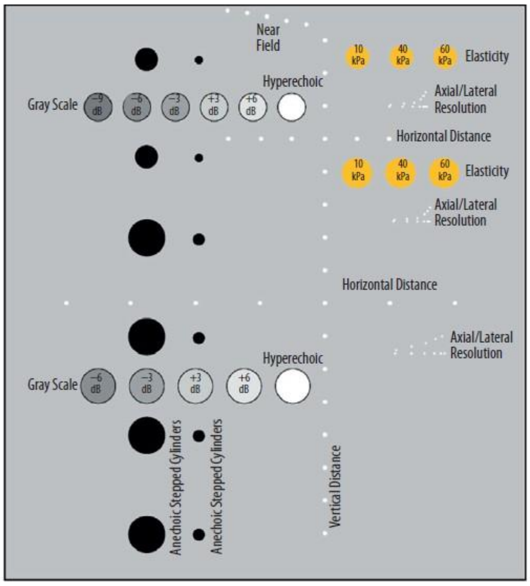


Fig. 4. A schematic for the phantom model CIRS 040GSE, Fabiszewska et al. (2017)

For data to be extracted, the stored DICOM images were uploaded to the open-source software ImageJ. A circular selection tool was used to draw a ROI on the targets. As shown in Fig. 5, the circular selection is represented in yellow. Data provided from the ROI includes the circular area, mean pixel value (MPV), SD, the maximum pixel value and the minimum pixel value. Four other ROIs were drawn around the target's background, and data was recorded for each ROI, as shown through Fig. 6, also in yellow. For most probes, this process was repeated for the targets at the depths of 3 cm and 11.5 cm within the phantom. Shown in Table III, the five data sets were noted for each target. The first one is that of the target itself, and the remaining four refer to data points of the target's background.

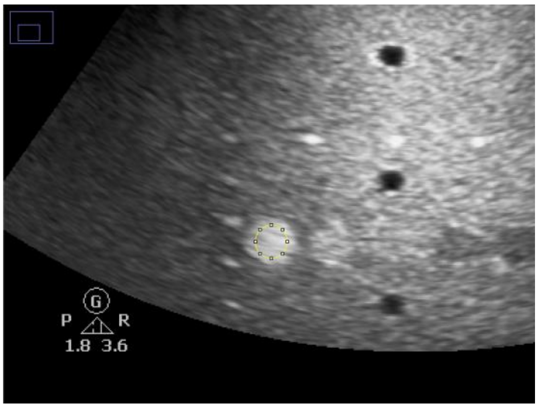


Fig. 5. Circular selection of a target at a depth of 11.5 cm in Image J

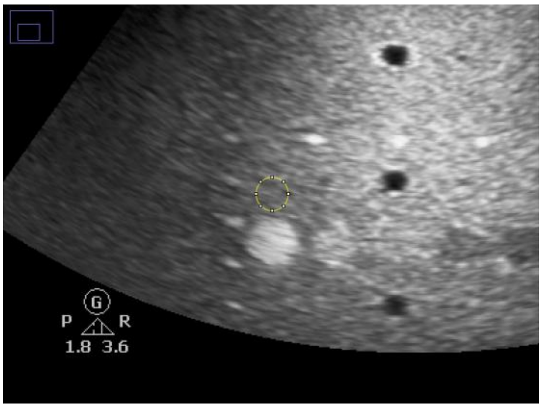


Fig. 6. Circular selection outside a target at a depth of 11.5 cm in Image J

Table III: Data of a curvilinear probe obtained through ImageJ Method 1 - Gamma Method:

| | |
|---|---|
| **Manufacturer and Model:** | Philips Sparq |
| **Probe Type and Name:** | Curvilinear - C5-1 |
| **Probe Central Frequency:** | 2 MHz |

| Depth (cm) | dB | Area | Mean | SD | Min | Max |
|---|---|---|---|---|---|---|
| | | 328 | 129.665 | 10.302 | 98 | 156 |
| | | 328 | 173.259 | 13.884 | 141 | 201 |
| 11.5 | -6 | 328 | 153.003 | 16.765 | 115 | 201 |
| | | 383 | 146.65 | 13.414 | 118 | 181 |
| | | 383 | 145.509 | 14.134 | 106 | 182 |
| | | 328 | 147.238 | 11.261 | 116 | 169 |
| | | 328 | 185.073 | 12.132 | 161 | 220 |
| 11.5 | -3 | 328 | 175.506 | 14.495 | 141 | 209 |
| | | 328 | 160.207 | 14.053 | 126 | 206 |
| | | 328 | 152.939 | 17.332 | 116 | 206 |
| | | 384 | 180.656 | 10.961 | 156 | 208 |
| | | 384 | 182.383 | 13.287 | 154 | 220 |
| 11.5 | 3 | 384 | 173.982 | 15.177 | 133 | 209 |
| | | 384 | 161.964 | 12.678 | 134 | 204 |
| | | 384 | 176.458 | 16.024 | 135 | 209 |
| | | 384 | 184.711 | 10.629 | 151 | 205 |
| | | 384 | 165.807 | 14.131 | 125 | 204 |
| 11.5 | 6 | 384 | 163.385 | 18.277 | 124 | 213 |
| | | 384 | 153.016 | 15.709 | 122 | 214 |
| | | 384 | 174.453 | 14.727 | 133 | 209 |
| | | 384 | 198.294 | 8.807 | 169 | 218 |
| | | 384 | 139.763 | 11.183 | 103 | 175 |
| 11.5 | 15 | 384 | 133.812 | 12.854 | 102 | 166 |
| | | 384 | 106.552 | 13.183 | 78 | 156 |
| | | 384 | 163.266 | 20.19 | 118 | 214 |

For this method to be explored, the MPV of each target, that is, the first MPV entry from Table III, was plotted as shown in dark blue in Fig. 7. In this way, the gradient, representing the gamma value, was obtained together with the $R^{!}$ value.

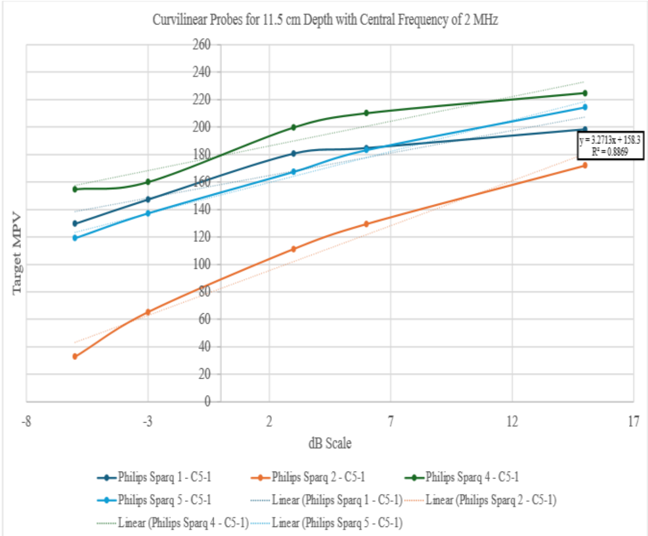


Fig. 7. A graph which represents the results of the gamma method for four curvilinear probes

Method 2 - IC Method: In the IC method also analysed by Gibson et al. (2001), the ratio of the mean of pixel values within the contrast region to those outside the contrast region was evaluated. Using the mean column in Table III, the IC for each target was calculated. As a result, the data as shown in Table IV was generated for each probe and depth.

Method 3 - CNR Method: For the CNR to be evaluated as suggested by Sanchez et al. (2009), the following equation was used.

$$\mathrm{CNR} = \frac{|\langle \mu_{\mathrm{B}} - \mu_{\mathrm{L}} \rangle|}{\left|\sqrt{\sigma_{\mathrm{B}}^2 + \sigma_{\mathrm{L}}^2}\right|} \tag{3.1}$$

From equation (3.1), $\mu_{\$}$ and $\mu_{\%}$ refer to the mean values of the background and target or lesion, respectively, whilst $\sigma_{\$}$ and $\sigma_{\&}$ represents the variance of the background and target/lesion, respectively. The CNR data also found in Table IV was obtained for a curvilinear probe at a depth of 11.5 cm.

This process was also repeated for every probe investigated. In hand with this, graphs similar to the one in Fig. 8 were generated for the remaining probes under investigation.

Table IV: The IC and CNR values for a curvilinear probe

| | | |
|---|---|---|
| **Manufacturer and Model:** | Philips Sparq | |
| **Probe Type and Name:** | Curvilinear - C5-1 | |
| **Probe Central Frequency:** | 2 MHz | |
| **Depth** | 11.5 cm | |
| **dB** | **IC** | **CNR** |
| -6 | 0.839 | 1.399 |
| -3 | 0.874 | 1.154 |
| 3 | 1.040 | 0.386 |
| 6 | 1.125 | 1.083 |
| 15 | 1.460 | 3.708 |

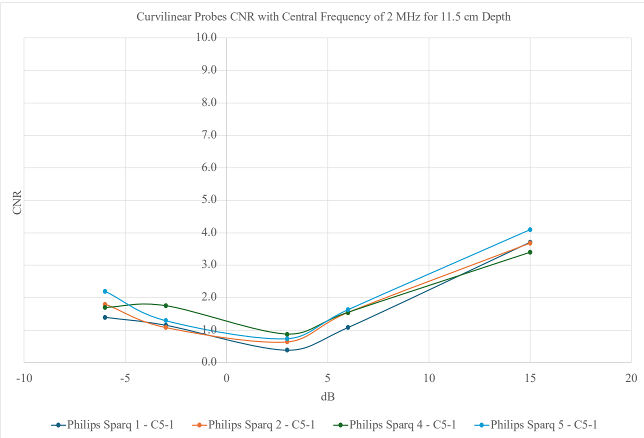


Fig. 8. A graph which represents the CNR of four curvilinear probes

## III. RESULTS & DISCUSSION

From the results generated, it is important to note that the linear probes under investigation were not evaluated at a depth of 11.5 cm. As highlighted by Vanderland and Kumar (2021), linear array probes operate at high frequencies and have a narrow beam, allowing detail to be achieved only at shallow depths. This is because, for deeper structures, less sound energy will be received due to the weak intensity echoes received by the transducers.

The contrast resolution was first investigated across different frequencies at the near field and far field zones. For the near field, at a depth of 3 cm, the linear, curvilinear and sector probes established distinctive features, even though in general, high IC was achieved in the hyperechoic structures. This relationship was also established in the study by Gibson et al. (2001). The IC values for the linear probes were similar across different central frequencies. With regards to the curvilinear and sector probes, even though the IC varied from 0 to 3, a steeper gradient was achieved in the sector probes. On the other hand, at a depth of 11.5 cm, the curvilinear probes with various central frequencies achieved better linearity except for the 5 MHz probe at the -6 dB (hypoechoic) target. Figs. 9 to 13 represent the abovementioned.

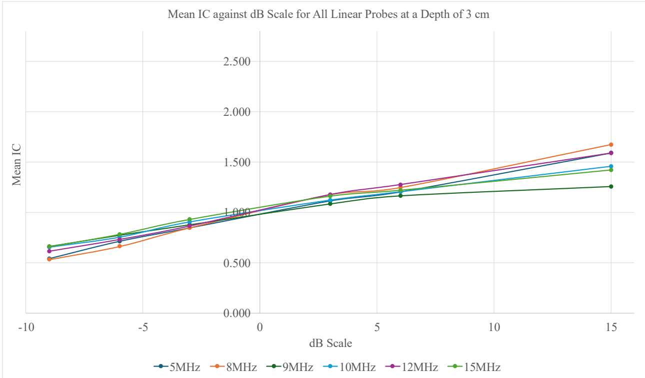


Fig. 9. Mean IC against dB scale for all linear probes at a depth of 3 cm

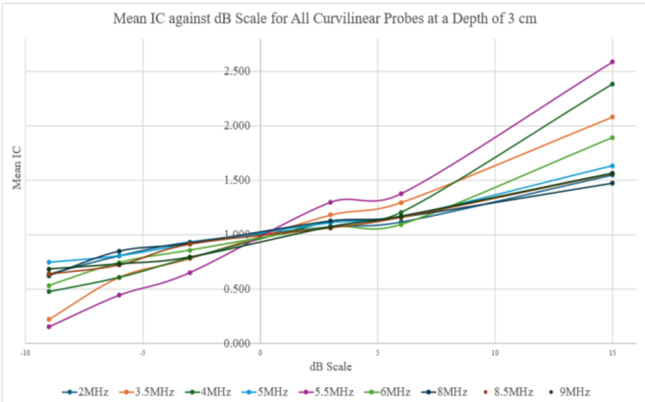


Fig. 10. Mean IC against dB scale for all curvilinear probes at a depth of 3 cm

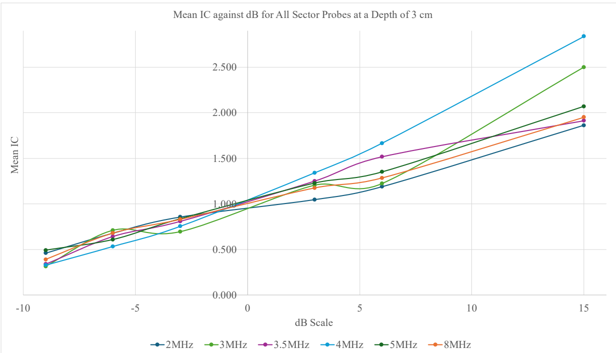


Fig. 11. Mean IC against dB scale for all sector probes at a depth of 3 cm

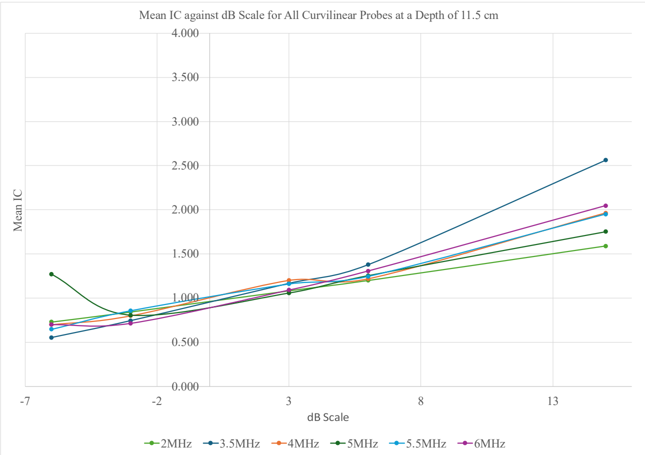


Fig. 12. Mean IC against dB scale for all curvilinear probes at a depth of 11.5 cm

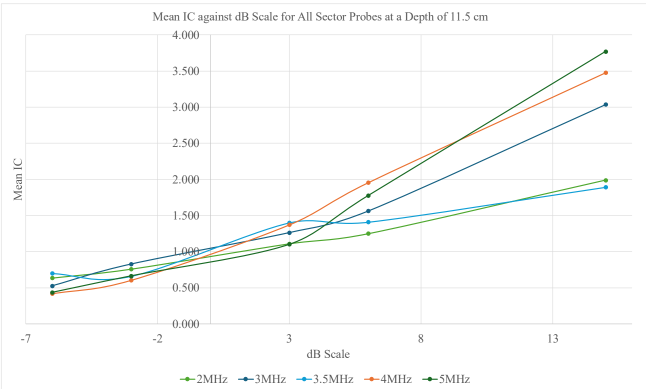


Fig. 13. Mean IC against dB scale for all sector probes at a depth of 11.5 cm

Since a limited number of probes were tested and averaged, improvements could have been made by taking repeated measurements. Moreover, since acceptance test images were subjectively obtained, different settings were used to achieve an optimized image which might have been affected by the amplification gain, TGC and focus.

With regards to the gamma of the system, as implied by Sharawy et al. (2016), if a large gamma value is obtained, a wider range of echo intensities are present within the available greyscale spectrum. This would lead to an increased contrast resolution.

Conversely, if a small gamma value is obtained, a narrower range of echo intensities are spread out across the greyscale spectrum, hence leading to poor contrast resolution. This explains why for both the near and far field, the sector probes established the best contrast resolution. On a similar note, no pattern was in general established on how the average gamma value varies across different frequencies.

For the $R^{!}$ value, given that most probes had values between 0.800 and 1.000, it ensures that the predictions are identical to the observed values. However, for the curvilinear probes with frequencies of 4 MHz and 8 MHz, an $R^{!}$ of approximately 0.700 was obtained, which could have been improved by taking repeated values. A summary of these values can be found in Tables V and VI.

Table V: A table summary of the gamma and $R^{!}$ values of all the probes investigated at a depth of 3 cm

| Average Gamma Value and Average | | for All Probes at 3 cm Depth!! | |
|---|---|---|---|
| | **Central Frequency (MHz)** | **Gamma Value** | !! |
| Linear | 5 | 3.554 | 0.934 |
| | 8 | 4.398 | 0.954 |
| | 9 | 2.949 | 0.858 |
| | 10 | 3.113 | 0.968 |
| | 12 | 4.611 | 0.948 |
| | 15 | 1.919 | 0.905 |
| Curvilinear | 2 | 3.562 | 0.867 |
| | 3.5 | 4.254 | 0.917 |
| | 4 | 2.069 | 0.718 |
| | 5 | 3.463 | 0.934 |
| | 5.5 | 4.355 | 0.999 |
| | 6 | 5.010 | 0.983 |
| | 8 | 4.004 | 0.770 |
| | 8.5 | 2.788 | 0.962 |
| | 9 | 2.700 | 0.979 |
| Sector | 2 | 5.086 | 0.977 |
| | 3 | 4.755 | 0.950 |
| | 3.5 | 3.937 | 0.996 |
| | 4 | 6.186 | 0.971 |
| | 5 | 4.672 | 0.955 |
| | 8 | 4.907 | 0.887 |

Considering the CNR investigated at a depth of 3 cm, the results generated for the linear probe imply that the higher the frequency, the smaller the CNR is across the echoic targets. A similar situation was achieved for the curvilinear probes; however the 6 MHz frequency achieved the lowest CNR at the +3 dB target. This is in agreement with Sassaroli et al. (2019). However, given that there was only one probe with such a frequency investigated in comparison to the majority of the curvilinear probes, some discrepancies might have resulted. Therefore, considering more probes will further confirm or deny such a statement. For the sector probes, the hypoechoic targets at high-frequency probes achieved a higher CNR but for the hyperechoic targets, no pattern was identified. In general, the sector probes established higher CNR values. At the far field, the sector probes yet again achieved higher CNR values in comparison to the curvilinear probes. Moreover, the sector probes allowed a better indication of how the CNR varies with higher frequencies at different targets. Except for the 3.5 MHz probe (in which only one probe was tested at this frequency), the CNR seemed to increase with increasing frequency. In the study by Sassaroli et al. (2019), it was also concluded that in the probes investigated (linear and convex), the CNR was better for the hypoechoic targets. The graphs generated for this method are represented through Figs. 14 to 18.

Table VI: A table summary of the gamma and $R^{!}$ values of all the probes investigated at a depth of 11.5 cm

| Average Gamma Value and Average | | for All Probes at 11.5 cm Depth | |
|---|---|---|---|
| | **Central Frequency (MHz)** | **Gamma Value** | $R^2$ |
| Curvilinear | 2 | 4.487 | 0.940 |
| | 3.5 | 5.509 | 0.964 |
| | 4 | 3.719 | 0.973 |
| | 5 | 5.034 | 0.989 |
| | 5.5 | 6.675 | 0.987 |
| | 6 | 4.264 | 0.995 |
| Sector | 2 | 5.892 | 0.983 |
| | 3 | 5.193 | 0.957 |
| | 3.5 | 4.085 | 0.969 |
| | 4 | 8.588 | 0.988 |
| | 5 | 6.540 | 0.917 |

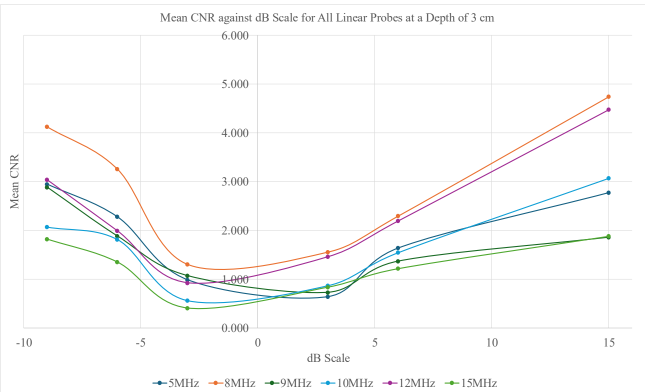


Fig. 14. Mean CNR against dB scale for all linear probes at a depth of 3 cm

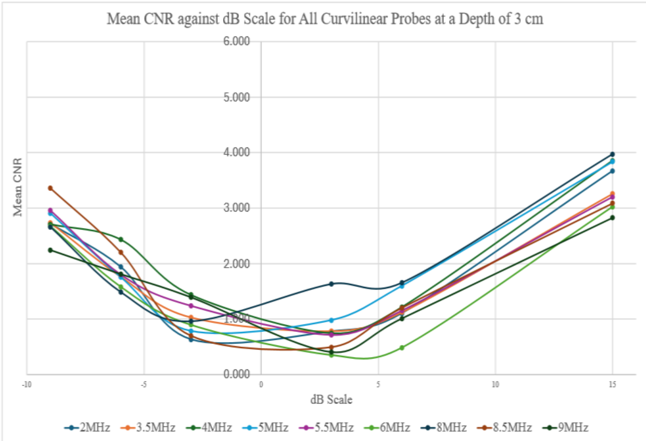


Fig. 15. Mean CNR against dB scale for all curvilinear probes at a depth of 3 cm

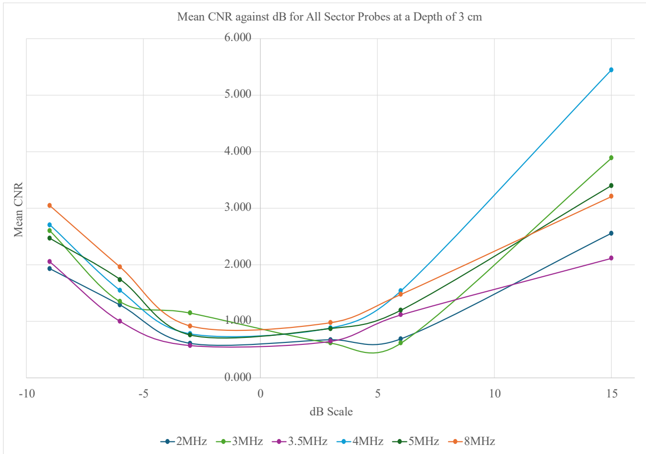


Fig. 16. Mean CNR against dB scale for all sector probes at a depth of 3 cm

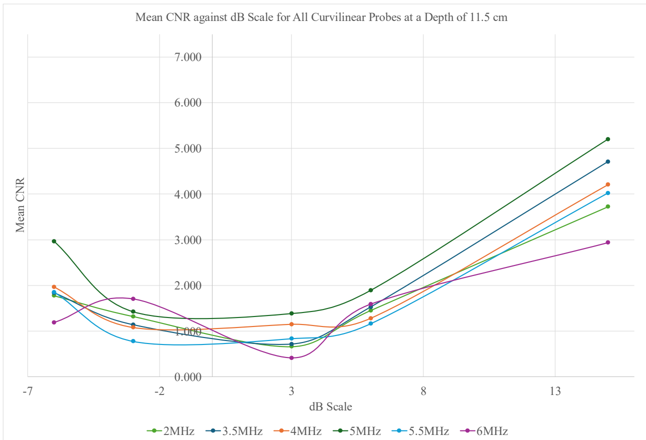


Fig. 17. Mean CNR against dB scale for all curvilinear probes at a depth of 11.5 cm

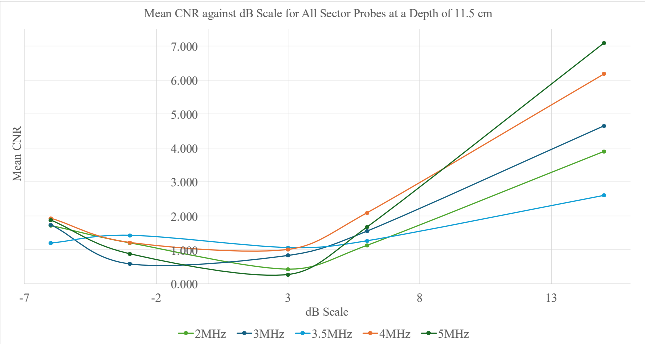


Fig. 18. Mean CNR against dB scale for all sector probes at a depth of 11.5 cm

The contrast resolution was then investigated across different transducers. This was done by taking a common frequency across all probe types, which was 5 MHz. The IC at the near field is quite similar for all probes. However, the 5 MHz curvilinear and sector probes established different characteristics for the far field zones as shown in Figs. 19 and 20.

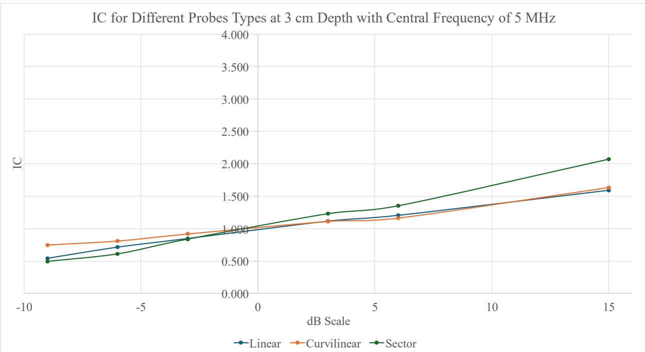


Fig. 19. Mean IC against dB scale for different probes with a common frequency of 5 MHz and at a depth of 3 cm

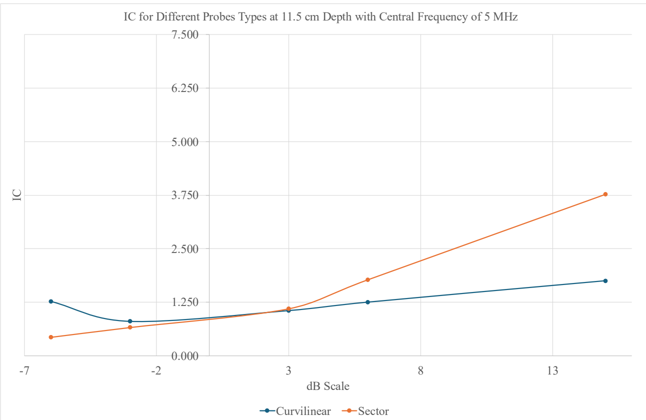


Fig. 20. Mean IC against dB scale for different probes with a common frequency of 5 MHz and at a depth of 11.5 cm

The curvilinear probes established a linear relationship from -3 to +15 dB targets whilst for the sector probes, a sharp gradient was achieved between the +3 dB and +6 dB targets. Through Tables VII and VIII, higher gamma values were obtained at 11.5 cm, indicating good contrast resolution.

Table VII: Gamma and $R^2$ values for different probes with a common frequency of 5 MHz and at a depth of 3 cm

| **Average Gamma Value and Average** | **for the 5 MHz Probes at 3 cm Depth** | |
|---|---|---|
| **Probe Type** | **Gamma Value** | **$R^2$** |
| Linear | 3.554 | 0.934 |
| Curvilinear | 3.463 | 0.934 |
| Sector | 4.672 | 0.955 |

Table VIII: Gamma and $R^1$ values for different probes with a common frequency of 5 MHz and at a depth of 11.5 cm

| **Average Gamma Value and Average** | **for the 5 MHz Probes at 11.5 cm Depth** | |
|---|---|---|
| **Probe Type** | **Gamma Value** | **$R^2$** |
| Curvilinear | 5.034 | 0.989 |
| Sector | 6.540 | 0.917 |

However, with regards to the $R^1$ values, all values were greater than 0.900. The CNR as shown in Figs. 21 and 22, established a similar shape. But, for the 11.5 cm depth, the sector probes established a steeper gradient between the +6 dB and +15 dB targets.

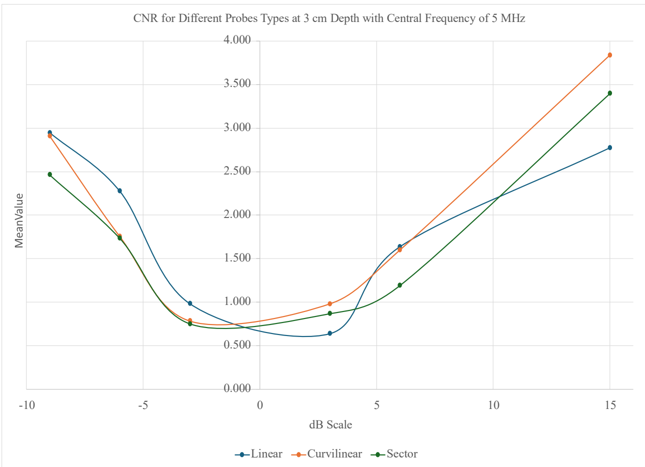


Fig. 21. Mean CNR against dB scale for different probes with a common frequency of 5 MHz and at a depth of 3 cm

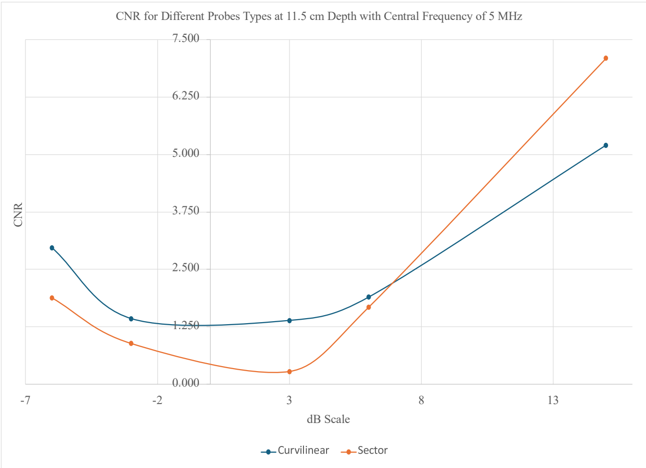


Fig. 22. Mean CNR against dB scale for different probes with a common frequency of 5 MHz and at a depth of 11.5 cm

Lastly, the contrast resolution was investigated by plotting Figs. 23 and 24, respectively. In both graphs, it was found that the values of the IC and CNR were higher at the 11.5 cm depth when compared to the 3 cm depth. With regards to such a characteristic, no literature was found. On the other hand, with regards to the gamma and the $R^1$ values, the same concept applies as discussed earlier.

Overall, the values obtained were quite consistent with the literature. With regards to the sector probes investigated in this study, steeper IC gradients and sharper U-shaped plots for the CNR were obtained. This is because the majority of the sector probes tested can operate in 3D. On a different note, it was noted that hyperechoic targets have higher contrast. Such a result was also achieved by Gibson et al.

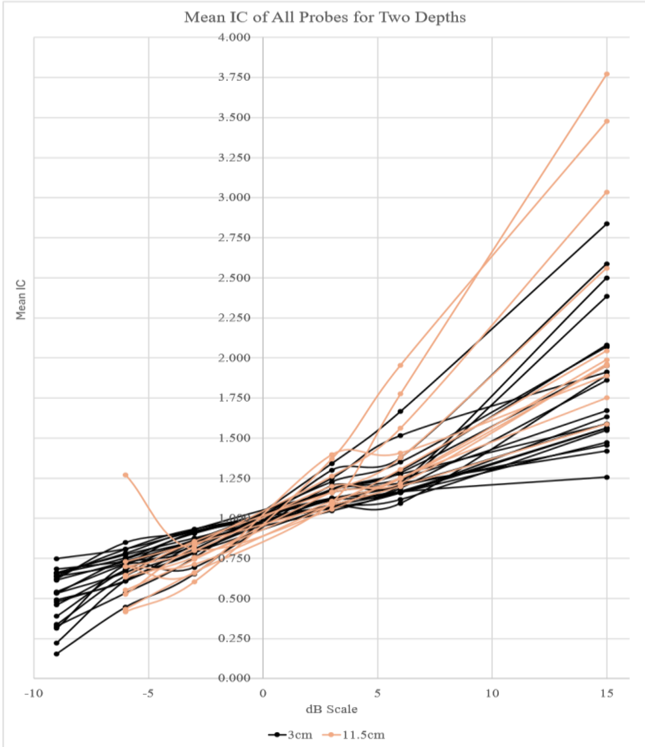


Fig. 23. Mean IC against dB scale for all probes at two different depths

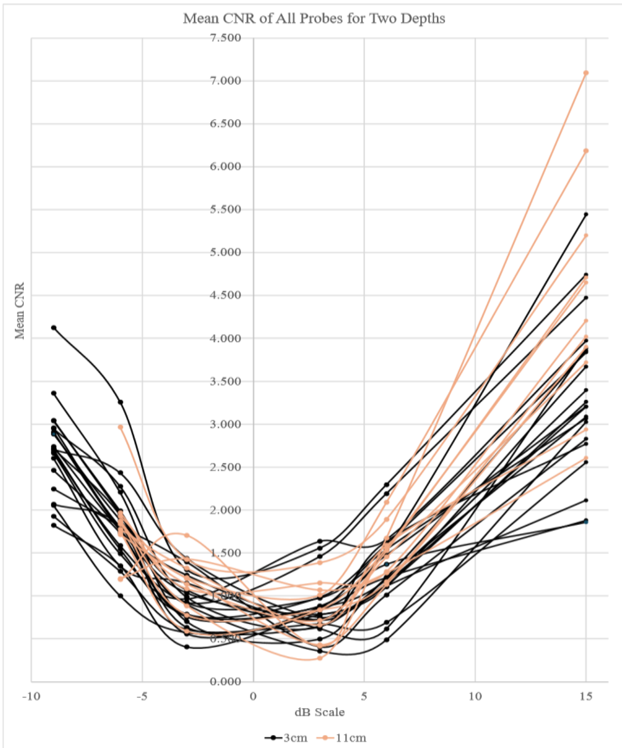


Fig. 24. Mean CNR against dB scale for all probes at two different depths

(2001). From the above-mentioned, it can be deduced that the gamma of the system does not depend on the frequency but rather on the probe.

Regarding the current guidelines established by the AAPM and IPEM 102, they do not provide any recommended action levels. Having said that, improvement and revision is necessary to minimise subjectivity and ensure that better protocols are in place.

Although this study thoroughly investigated three quantitative methods, there is still room for improvement. By considering more US systems and probes, better averaged data would be obtained, in turn offering better indication of how the contrast resolution varies with different frequencies and probes. On another note, upon selecting the ROIs on ImageJ, having equal areas will ensure that the data extracted is more precise and accurate, ensuring repeatability. The study could also be improved by investigating how different US systems establish different IC, gamma and CNR values. This would allow the MPs to compare which system performs better, which in turn can help them in the procurement process and testing.

## IV.CONCLUSION

The main conclusions of the study were:

- For all transducer types, it was noted that the IC increases with hyperechoic structures, establishing a linear relationship.
- All transducer types established characteristic U- shaped scatter plots for the CNR which is in agreement with Sassaroli et al. (2019).
- All probes had varying gamma values. However, it was noted that it depends on the type of transducer, not on the frequency.
- Overall, the sector probes established a better contrast resolution performance for both the near and far field zones.
- From most data plotted, it was noted that the contrast resolution is not frequency dependent.

Suggestions for further research are:

- Repeating the study with more US systems and US probes will allow the full frequency range at which the US systems operate to be investigated.
- Equal areas of circular selection will increase repeatability.
- Besides using images from acceptance testing, images from various QC procedures can be investigated to evaluate thoroughly how the US systems and probes perform over the years.

## REFERENCES


[1] Lanzolla, A. M. L., Andria, G., F. Attivissimo, G. Cavone, & Giaquinto, N. (2011). Improving B-mode ultrasound medical images. https://doi.org/10.1109/imtc.2011.5944261.

[2] CIRS. (n.d.). Multi-Purpose, Multi-Tissue Ultrasound Phan- tom. CIRS Product Support. Retrieved April 21, 2024, from https://support.cirsinc.com/product/multi-purposemulti- tissue-ultrasound-phantom/

[3] Fabiszewska, E., Pasicz, K., Grabska, I., Skrzynski, W., Slusarczyk-Kacprzyk, W., & Bulski, W. (2017). Evaluation of Imaging Parameters of Ultrasound Scanners: Baseline for Future Testing. Polish Journal of Radiology, 82, 773–782. https://doi.org/10.12659/pjr.904135

[4] Gibson, N. M., Dudley, N. J., and Griffith, K. (2001). A computerised quality control testing system for b-mode ultrasound. Ultrasound in Medicine Biology, 27:1697–1711.

[5] Sanchez, J. R., Pocci, D., and Oelze, M. L. (2009). A novel coded excitation scheme to improve spatial and contrast resolution of quantitative ultrasound imaging. IEEE Transactions on Ultrasonics, Ferroelectrics, and Frequency Control, 56:2111–2123.

[6] Sassaroli, E., Crake, C., Scorza, A., Kim, D., and Park, M. (2019). Image quality evaluation of ultrasound imaging sys- tems: advanced b-modes. Journal of Applied Clinical Medical Physics, 20:115–124.

[7] Vanderland, M., & Kumar, T. (2021). Point-of-Care Ultrasound for Outpatient Neurology. Practical Neurology. https://practicalneurology.com/articles/2021-nov-dec/pointof- care-ultrasound-for-outpatient-neurology



Contacts of the corresponding author:

Author: Kelsey Ann Micallef
Institute: University of Malta
City: Msida
Country: Malta
Email: kelsey.micallef.20@um.edu.mt